Heliyon 10 (2024) e31973

Contents lists available at ScienceDirect

Heliyon

journal homepage: www.cell.com/heliyon

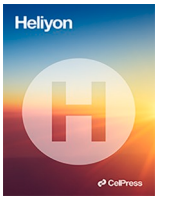

Research article

# GGTLC1 knockdown inhibits the progression of endometrial cancer by regulating the TGF-β/Smad signaling pathway

Xiaolin Tang [a,b,c,d], Xuehan Bi [a,c,d], Aihong Yang [a,c,d], Qinganzi Wang [a,c,d], Yongxiu Yang [a,c,d,*,1]

[a] The First School of Clinical Medicine, Lanzhou University, Lanzhou, 730099, China
[b] The Third People's Hospital of Gansu Province, Lanzhou, China
[c] Department of Obstetrics and Gynecology, The First Hospital of Lanzhou University, Lanzhou, China
[d] Key Laboratory for Gynecological Oncology Gansu Province, Lanzhou, China

ARTICLE INFO

*Keywords:*
GGTLC1
Endometrial cancer
TGF-β/Smad signaling pathway
Transcriptome sequencing
Immune infiltration

ABSTRACT

*Purpose:* Endometrial cancer (EC) poses a serious risk to females worldwide; thus, a deep understanding of EC is urgently required. The role and mechanisms of gamma-glutamyltransferase light chain 1 (GGTLC1) in EC remain obscure. This study aims to elucidate the function and mechanisms underlying GGTLC1's involvement in EC.

*Methods:* Bioinformatic tools and databases were used to analyze GGTLC1 and its associated gene expression in EC tissues. Functional enrichment explorations and immune infiltration analyses were conducted, together with investigation into the methylation status of GGTLC1. Western blotting and Quantitative real-time PCR quantified expression levels. Additional experimental methodologies elucidated the role of GGTLC1 in EC progression. Transcriptome sequencing identified potential regulatory pathways for GGTLC1, and tumor growth was evaluated in vivo using HEC-1A cells in nude mice.

*Results:* GGTLC1 was upregulated and negatively correlated with immune cell infiltration and DNA methylation in EC. Cell migration and proliferation were reduced following GGTLC1 knockdown, together with arrest at the G0/G1 phase and an upsurge in apoptosis. Compared to the knockdown group, TGF-β/Smad signaling pathway was up-regulated in the negative control group of EC cells by transcriptome analysis. The levels of TGF-β, pSmad2, and pSmad3 followed the same decreasing trend, whereas Smad3 and Smad2 protein levels remained unchanged.

*Conclusion:* Knockdown of GGTLC1 attenuates EC development through the TGF-β/Smad pathway, positioning GGTLC1 as a promising target for EC treatment.

## 1. Introduction

Endometrial cancer (EC) represents a prevalent gynecological malignancy [1]. Although the majority of EC patients are diagnosed early and effectively treated with surgical interventions, managing advanced stages of the disease poses significant challenges [2,3]. Additionally, negative changes in diet and lifestyle have increased the prevalence of EC [4]. Hence, innovative approaches are urgently

* Corresponding author. The First School of Clinical Medicine, Lanzhou University, Lanzhou, 730099, China.
*E-mail address:* yxyanglzu@163.com (Y. Yang).
[1] Lead Contact. The First School of Clinical Medicine, Lanzhou University, Lanzhou, 730099, China.

https://doi.org/10.1016/j.heliyon.2024.e31973
Received 3 January 2024; Received in revised form 21 May 2024; Accepted 24 May 2024
Available online 25 May 2024

required to better diagnose and treat patients with EC.

The protein coding gene gamma-glutamyltransferase light chain 1 (GGTLC1), with a molecular mass of 24,274 Da, was initially named GGTL6, then GGTLA4, and later GGTLC1 in 2008 [5]. Members of the gamma-glutamyl transferase family, including GGTLC1, are critical in glutathione metabolism. Gamma-glutamyltransferase (GGT) is involved in various diseases, including cancer [6]. Serum GGT is a genitourinary malignancy predictive biomarker [7]. A recent study proposed the use of GGT-triggered charge-reversal nanoparticles as a cutting-edge drug for successful GGT-positive tumor treatment [8]. GGT has also been reported in other cancers [9–11]. Additionally, gamma-glutamyltransferase 1 (GGT1) is an important paralog of this gene. GGT1 inhibition can reduce the increased immunosuppressive activities of myeloid-derived suppressor cells (MDSCs) that are triggered by granulocyte colony-stimulating factor (G-CSF), ultimately counteracting tumor-promoting effects caused by G-CSF [12]. In renal carcinoma, GGT1 inhibition can inhibit proliferation and migration, induce cell cycle arrest, and improve sensitivity to chemotherapy [13]. Another study concluded that GGTLC1 produces chemoresistance in breast cancer through an immune pathway [14]. Our analysis of data from The Cancer Genome Atlas (TCGA) indicates the notable increase in GGTLC1 levels observed in EC.

TGF-β is overproduced across almost all types of advanced human tumors, and higher TGF-β expression promotes tumor growth and metastasis via increased tumor cell motility [15]. Earlier researches have indicated that the TGF-signaling pathway acts as a crucial role in EC development. In the human EC cell line (Ishikawa), fluorene-9-bisphenol (BHPF) has been shown to inhibit epithelial–mesenchymal transition (EMT) by blocking the pathway [16]. In the progression of esophageal squamous cell carcinoma (ESCC), ATAD2 collaborates with C/EBPβ to facilitate metastasis through the TGF-β1/Smad3 signaling pathway [17].

Our study explores the effects, and potential mechanisms, of GGTLC1 on EC cell biological actions, with the aim of proposing a novel treatment strategy for EC.

## 2. Materials and methods

### 2.1. Differentially expressed gene (DEG) and enrichment analyses

The RNA-sequencing data in FPKM format was obtained from the UCEC project of TCGA, available at https://portal.gdc.cancer.gov/. The data in HTSeq-FPKM format at level 3 were normalized to TPM. To analyze differentially expressed genes (DEGs) between the two groups, we utilized the DESeq2 R package version 1.26.0. DEGs were defined with adjusted p-value (p.adj) $< 0.05$ and $|\log2\text{-fold-change (FC)}| > 1$. Spearman's correlation analysis assessed the relationship between the expression of the top ten DEGs and GGTLC1. GO and KEGG analyses were conducted utilizing ClusterProfiler R package version 3.14.3.

### 2.2. DNA methylation and immune infiltration analyses

By utilizing MethSurv and UALCAN databases, methylation status of the GGTLC1 promoter was examined to investigate the underlying mechanism of GGTLC1 on ECs. An analysis of immune cell infiltration for GGTLC1 was conducted utilizing the GSVA package (version 1.34.0) in R to perform single-sample Gene Set Enrichment Analysis (ssGSEA). This analysis quantified the infiltration levels across 24 distinct immune cell types. Spearman's correlation analysis was employed to explore the relationships between GGTLC1 expression and the prevalence of these immune cells. Additionally, the Wilcoxon rank sum test was utilized to compare immune cell infiltration between EC samples with high and low GGTLC1 expression.

### 2.3. Patients and endometrial tissue samples

All patients provided their informed consent, and this study received approval from ethics committee of Lanzhou University School of Basic Medicine. Six patients who underwent hysterectomy at our hospital provided six pairs of EC tissues and associated paracancerous tissues. Prior to the surgery, none of these patients had received chemotherapy or radiation therapy.

### 2.4. Cell culture

Human endometrial epithelial cell (hEEC) line was obtained from Biobw (Beijing, China). Additional cell lines, including AN3CA, KLE, HEC-1B, Ishikawa, RL95-2, and HEC-1A, were sourced from Genechem Co., Ltd. The culture conditions varied according to the cell line: hEEC, Ishikawa, and RL95-2 cells were cultured in Dulbecco's Modified Eagle Medium (DMEM); AN3CA cells in Minimal Essential Medium (MEM); KLE cells in DMEM-F12; and both HEC-1A and HEC-1B cells in McCoy's 5A medium. Each medium was supplemented with 10 % fetal bovine serum (BI, Israel) and 1 % penicillin/streptomycin (Hyclone, USA).

### 2.5. shRNAs transfection and lentivirus infection

Short hairpin RNA (shRNA) constructs targeting specific genetic sequences were designed and synthesized by Shanghai Genachem Co., Ltd. The targeted gene or shRNA sequence was cloned into a lentiviral expression vector. For viral particle production, this vector was co-transfected with lentiviral backbone and packaging plasmids into a packaging cell line. Following transfection, the culture supernatant containing the lentiviral particles was harvested. HEC-1A cells were then infected with these lentiviruses; polybrene was added to enhance the infection efficiency. Post-infection, cells were selected with puromycin to establish stable lines. The success of lentiviral transduction was subsequently confirmed via Western blot analysis.

### 2.6. Quantitative real-time PCR (qRT-PCR)

Total RNA was isolated from cells using TRIzol reagent (Takara, Japan). RNA concentration and purity were assessed with a spectrophotometer. Complementary DNA (cDNA) synthesis was carried out using the PrimeScript RT kit (Cat. RR047A, TaKaRa) at 37 °C for 15 min, followed by a heat inactivation step of the reverse transcriptase at 85 °C for 5 s. A reaction mixture for quantitative real-time PCR (qRT-PCR) was prepared, including specific primers, an appropriate amount of cDNA template, and SYBR Green (Cat. RR820A, Takara). The qRT-PCR protocol included an initial denaturation at 95 °C for 30 s, followed by 40 cycles of denaturation at 95 °C for 5 s, and annealing/extension at 60 °C for 30 s. Relative gene expression levels were quantified using the comparative Ct method ($2^{\hat{}-\Delta\Delta Ct}$). The primers for GGTLC1 were as follows: F 5'-AAGCCCGAGTTCTACATGCC-3', R: 5'-GGTGATGCTGGTAGAGCTGA-3'; and for GAPDH: F: 5'-CAACGAATTTGGCTACAGCA-3', R: 5'-AGGGGAGATTCAGTGTGGTG-3'.

### 2.7. Western blot (WB) analysis

For protein extraction, samples of cells and tissues were gathered and lysed in RIPA buffer (Solarbio, Beijing, China) with protease and phosphatase inhibitors. The concentration of protein was determined utilizing a BCA protein assay kit (Solarbio, Beijing, China). Subsequently, the protein supernatants were mixed with 5 × SDS loading buffer and heated at 100 °C for 10 min. After that, the same amount of protein was separated using SDS-PAGE and transferred to polyvinylidene fluoride membranes. The membranes were then exposed to primary antibodies overnight at 4 °C and secondary antibodies for 1 h at room temperature. The primary antibodies that were employed are as follows: rabbit anti-GGTLC1 (1:1000, Signalway Antibody, cat. no. 40020), rabbit anti-pSmad2 (1:1000, Cell Signaling Technology, cat. no. 3108S), rabbit anti-Smad2 (1:1000, Cell Signaling Technology, cat. no. 5339S), rabbit anti-pSmad3 (1:2000, Boster Biological Technology, cat. no. BM4033), rabbit anti-Smad3 (1:2000, Boster Biological Technology, cat. no. BM3919), rabbit anti-TGF-β1/2 (1:1000, Beyotime Biotechnology, cat. no. AF0297), rabbit anti-caspase3 (1:1000, HuaBio, China, cat. no. ET1602-39), rabbit anti-bax (1:5000, HuaBio, China, cat. no. ET1603-34), rabbit anti-p21 (1:1000, Wanlei, China, cat. no. WL0362), rabbit anti-bcl2 (1:1000, HuaBio, China, cat. no. ET1702-53). The horseradish peroxidase-conjugated goat anti-rabbit IgG secondary antibody (Abbkine, cat. no. A21020) was used at a dilution of 1:10,000. Signal blots were detected utilizing the BeyoECL Moon kit.

### 2.8. Cell proliferation assay

Cell proliferation was quantified using the Cell Counting Kit-8 (CCK-8, BioScience, Shanghai, China). HEC-1A cells were seeded at a density of $5 \times 10^{\hat{}3}$ cells/100 μL per well in 96-well plates. Absorbance at 450 nm was measured to assess cell viability, comparing values between treatment and control groups to calculate relative changes in proliferation rate or cell activity. Cells were maintained in incubators at 37 °C with 5 % CO2.For colony formation assays, cells were plated at a density of $1 \times 10^{\hat{}3}$ cells per well in 6-well plates and cultured for two weeks to allow for colony development. Colonies were fixed with 4 % paraformaldehyde for 20 min and stained with 0.5 % crystal violet (Beyotime Biotechnology) for 30 min. Colony counts were manually performed from photographs. Additionally, cell proliferation was evaluated using the EdU incorporation assay with the Cell Proliferation EdU Image Kit (Abbkine, Wuhan, China) following the manufacturer's instructions. Fluorescent images were captured with a fluorescence microscope. All experiments were independently repeated in triplicate.

### 2.9. Cell migration assay

The migratory capacity of cells was investigated through wound healing and Transwell migration assays. Briefly, a wound healing assay was conducted by seeding cells into 6-well plates and culturing them to subconfluence. To scratch the cells, a sterile 200 μL pipette tip was utilized, followed by serum-free culture medium. Migration areas were monitored and imaged with an inverted microscope at 100× magnification at 0, 24, 48, and 72 h post-scratch. The areas were quantified using ImageJ software.

The Transwell migration assay was implemented in 6.5 mm polycarbonate inserts with 8.0 pore size (Costar Corning, New York, NY, USA). $2 \times 10^5$ cells per well were seeded into the upper chamber with 200 μL serum-free medium, while 600 μL medium containing 20 % fetal bovine serum (FBS) was used in the lower chamber. Fixing the cells with 4 % paraformaldehyde and staining them with 0.5 % crystal violet took place after 48 h of culture. We counted the cells from five random fields captured by an inverted microscope (magnification, 200 × ). All experiments were independently repeated in triplicate.

### 2.10. Flow cytometric analysis

Cells were collected using cell scraping and then treated with fixatives such as formaldehyde to ensure long-term preservation. Cells were fixed according to standardized protocols before being harvested for further processing. Cells were stained with propidium iodide following the manufacturer's guidelines. Post-staining, cells were washed with a flow-through buffer containing 2 % FBS to remove excess dye. The cell suspensions were then filtered through a 70-μm filter to eliminate aggregated cells and large debris. Cell concentrations were adjusted to $10^{\hat{}5}$ cells/ml, optimizing conditions for flow cytometric analysis. Flow cytometry was employed to assess cell cycle progression, apoptosis, and mitochondrial membrane potential. Cell cycle analysis was conducted using the Cell Cycle Analysis Kit (China United Branch). Apoptosis was evaluated using an Apoptosis Kit (China Union Branch), where cells were stained with Annexin V-FITC and PI following the provided protocol. Additionally, mitochondrial membrane potential was measured with the

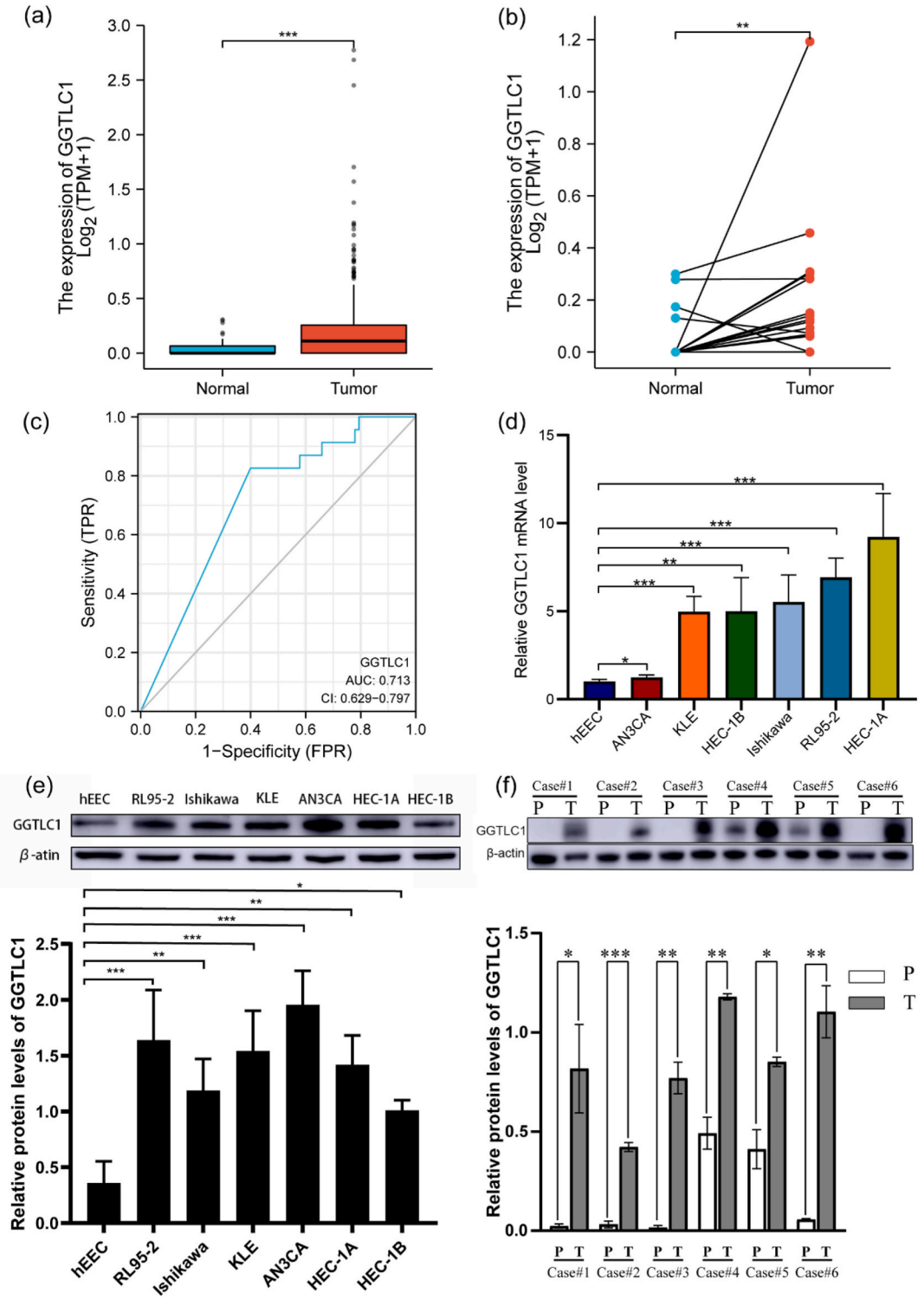


**Fig. 1.** Expression levels of GGTLC1 in EC. **a** GGTLC1 expression between EC and normal tissues in TCGA database (normal = 35, tumor = 543). **b** GGTLC1 expression between EC and adjacent normal endometrial tissues in TCGA database (normal = 23, tumor = 23). **c** ROC curve of GGTLC1 in EC from TCGA database. **d** qRT–PCR result of GGTLC1 mRNA expression in hEEC and six endometrial cancer cell lines. **e** Western blot analysis of the expression of GGTLC1 in hEEC and six endometrial cancer cell lines. **f** Western blotting of GGTLC1 expression in six fresh primary EC tissues (T) and individual normal para-cancerous tissues (P). *p < 0.05, **p < 0.01, and ***p < 0.001. Each experiment was repeated at least three times, statistical difference analysis was applied using either paired *t*-test or one-way analysis of variance test. The raw data of WB can be found in the supplementary file's Fig. 1(e) and (f).

JC1 Mitochondrial Membrane Potential Assay Kit (Biotech, Shanghai, China). All assays were conducted in triplicate to ensure reliability. Flow cytometry data were acquired and analyzed using NovoExpress software (version 1.5.6).

### 2.11. *In vivo tumor xenograft mouse model*

The Animal Ethics Committee of the School of Basic Medicine at Lanzhou University approved all experimental protocols involving animals. Four-week-old female BALB/c nude mice were sourced from the Shanghai Model Biology Center and housed in a specific pathogen-free (SPF) environment. The mice were randomly assigned to three groups (n = 5 per group): shNC, shGGTLC1-1, and shGGTLC1-2, to assess the impact of GGTLC1 knockout on HEC-1A cells in vivo. Each mouse received a subcutaneous injection of approximately $1.0 \times 10^{\hat{}7}$ exponentially growing HEC-1A cells suspended in 200 μL of phosphate-buffered saline (PBS) into the left axilla. Tumor growth was monitored at intervals of 48–72 h, and tumor volume was calculated using the formula: V = (length × width$^{\hat{}2}$)/2. On day 30, the mice were humanely euthanized, and the tumors were excised, evaluated, and photographed.

### 2.12. *Transcriptome sequencing*

Upon request, we prepared samples from HEC-1A shNC cells and shGGTLC1-2 cells, each with three independent biological replicates. These samples were sent to Shanghai Genecham Co., Ltd. for transcriptome sequencing. Total RNA was extracted using RNA extraction kits, including options such as TRIzol and Qiagen RNeasy. The quality and concentration of the extracted RNA were assessed using a NanoDrop system. RNA purification involved the use of oligo(dT) beads to isolate mRNA or total RNA, which was then fragmented at high temperatures into lengths of 200–500 bases, suitable for sequencing. RNA was reverse transcribed into cDNA using random or oligo(dT) primers. Single-stranded cDNA was synthesized into double-stranded cDNA using DNA polymerase and RNase H. The cDNA ends were then blunted and phosphorylated. An 'A' tail was added to the 3′ ends of the cDNA to facilitate the ligation of sequencing adapters. Specific sequencing linkers were then attached. The appropriate length of cDNA fragments was selected using gel electrophoresis or magnetic beads. The cDNA library was amplified by PCR to ensure there was sufficient material for sequencing. The prepared library was loaded onto an Illumina platform for single-end sequencing. Initial processing of the raw sequencing data involved removing low-quality reads. Reads were aligned to the reference genome or transcriptome using HISAT2. Gene expression levels were quantified using Feature Counts.

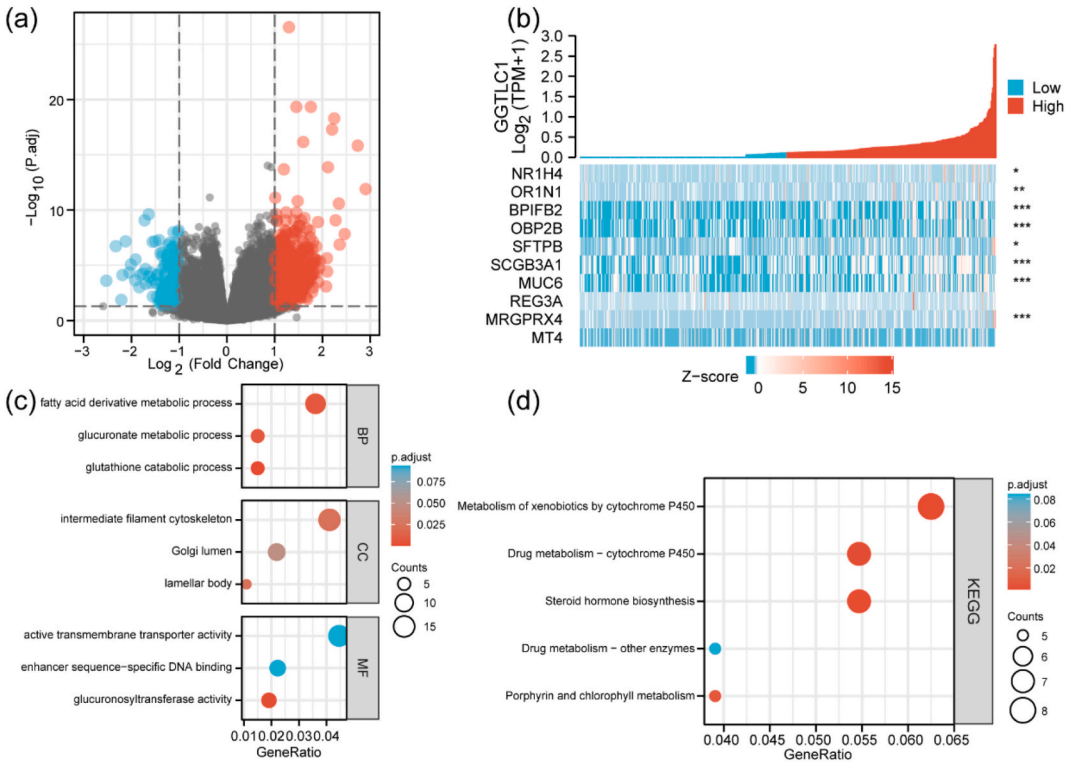


**Fig. 2.** Differentially expressed genes (DEGs) and functional enrichment analysis (GO and KEGG) of GGTLC1 in EC. **a** Volcano plot of differentially expressed genes (DEGs). **b** Heatmap of correlation between GGTLC1 expression and the top ten DEGs. **c** GO enrichment analysis of DEGs. d KEGG pathway annotation of DEGs.

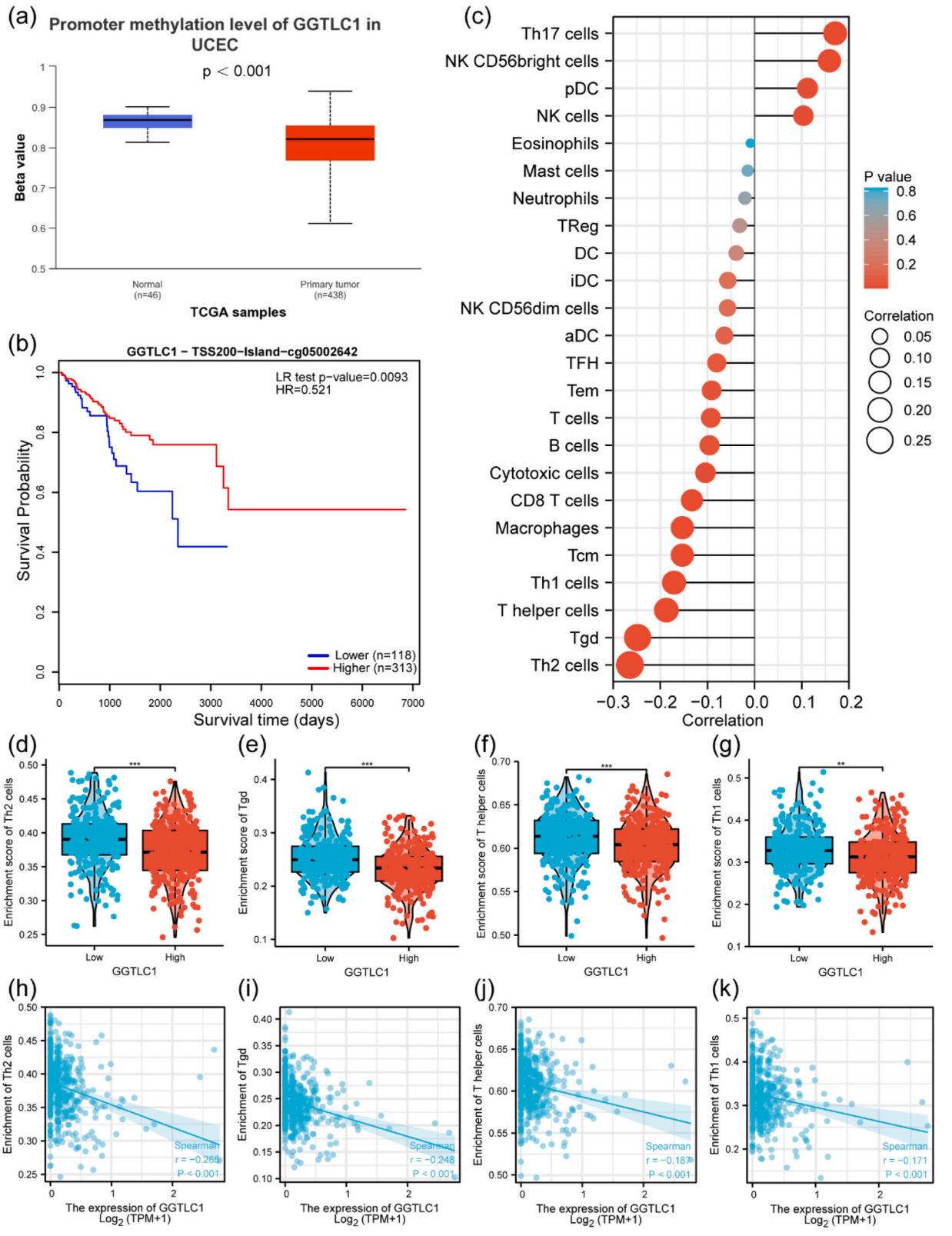


(caption on next page)

**Fig. 3.** Correlation between GGTLC1 expression and methylation and immune infiltration levels in endometrial cancer. **a** The promoter methylation level of GGTLC1 in endometrial cancer was obtained from the UALCAN database. **b** Kaplan–Meier survival curve for the GGTLC1 methylation site cg05002642. **c** Correlation between GGTLC1 expression and 24 types of immune cells. The size of the point represents the corresponding absolute values of Spearman's correlation coefficient. **d–g** Comparison of immune infiltration levels of immune cells, including Th2 cells, Tgds, T helper cells, and Th1 cells, between the high- and low-GGTLC1 expression groups. **h–k** Correlation between GGTLC1 expression and the relative enrichment scores of immune cells (including Th2 cells, Tgds, T helper cells, and Th1 cells).

### 2.13. Statistical analyses

Three independent experiments were performed for each analysis. R 3.6.3 or SPSS 26.0 was utilized to perform statistical analysis. One-way ANOVA was utilized to compare factors between groups. The interaction between GGTLC1 expression and DEGs or immune infiltrating cells was investigated utilizing Spearman's correlation analysis.Kaplan-Meier survival analysis was performed utilizing the 'survival' package in R to estimate survival probabilities at designated time points. The log-rank test was applied to compare survival curves statistically across different groups, determining the significance of differences in survival outcomes. The Receiver Operating Characteristic (ROC) analysis was performed using the pROC package in R. The effectiveness of the test was quantified by the area under the curve (AUC). An AUC value close to 1 indicates excellent test performance, suggesting high diagnostic accuracy, whereas a value near 0.5 implies that the test has no diagnostic value.

## 3. Results

### 3.1. GGTLC1 is upregulated in EC

Comparing EC tissues to normal tissues, GGTLC1 expression was greater in the EC tissues analyzed using TCGA database ($p < 0.001$) (Fig. 1a), which was consistent with the results observed in the 23 paired samples (Fig. 1b). In addition, the receiver operating characteristic (ROC) curve showed that the ability of GGTLC1 expression to discriminate between EC tissues and normal tissues was moderate. The area under the curve (AUC) was 0.713 (95 % confidence interval [CI]: 0.629 − 0.797) (Fig. 1c). Compared to hEEC cells, the levels of GGTLC1 expression in EC cells, including AN3CA, KLE, HEC-1B, Ishikawa, RL95-2, and HEC-1A, were noticeably increased ($p < 0.05$; Fig. 1d and e). In primary EC tissue samples, GGTLC1 protein expression was markedly increased compared to that in normal paracancerous tissues ($n = 6$, $p < 0.05$; Fig. 1f).

### 3.2. DEG and functional enrichment analyses of GGTLC1 in EC

By analyzing GGTLC1 expression levels, a total of 1108 DEGs were identified as either up- or downregulated, including 928 up- and 180 downregulated genes ($|\log_2 FC| > 1$ and adjusted p-value $<0.05$) (Fig. 2a). The top ten DEGs of the correlation heatmap are displayed (NR1H4, OR1N1, BPIFB2, OBP2B, SFTPB, SCGB3A1, MUC6, REG3A, MRGPRX4, and MT4), as well as GGTLC1 (Fig. 2b). Following this, GO enrichment analysis displayed the top GO enrichment items as follows: fatty acid derivative metabolic process, glucuronate metabolic process, glutathione catabolic process, intermediate filament cytoskeleton, Golgi lumen, lamellar body, active transmembrane transporter activity, enhancer sequence-specific DNA binding, and glucuronosyltransferase activity (Fig. 2c). Next, KEGG pathway analysis of DEGs identified several significant enrichments (Fig. 2d), including steroid hormone biosynthesis, metabolism of xenobiotics by cytochrome P450, and drug metabolism-cytochrome P450.

### 3.3. Relationship between GGTLC1 expression and immune infiltration and methylation

The relationship between GGTLC1 expression and methylation was investigated using the UALCAN database. Compared to normal endometrial tissues, EC tumor tissues displayed a strikingly decreased degree of DNA methylation ($p < 0.001$; Fig. 3a). The methylation site cg05002642 indicated a poor prognosis in EC (Fig. 3b). Furthermore, we found an inverse relationship between GGTLC1 expression and immune cell infiltration levels, including Th2 cells ($r = -0.265$, $p < 0.001$), T gamma delta (Tgd) cells ($r = -0.248$, $p < 0.001$), T helper cells ($r = -0.187$, $p < 0.001$), and Th1 cells ($r = -0.171$, $p < 0.001$) (Fig. 3c). The GGTLC1 high-expression group had lower enrichment scores for Th2 cells, Tgds, T helper cells, and Th1 cells than the GGTLC1 low-expression group (all $p < 0.01$) (Fig. 3d–k).

### 3.4. GGTLC1 knockdown reduced the capacity of EC cells to proliferate and migrate in vitro

To elucidate the role of played in EC development and progression, we employed three lentiviral shRNAs to reduce GGLTC1 expression in HEC-1A cells, while empty lentiviral vectors were used as negative controls. The transfection effectiveness was validated by western blotting (Fig. 4a and b). As a result, shGGTLC1-1 and shGGTLC1-2 were selected for the following experiments. Silencing of GGTLC1 slowed HEC-1A cell growth, which was identified through CCK8, colony formation, and EdU experiments (Fig. 4c–g). We found that GGTLC1 knockdown also caused a decrease in the migration capacity of HEC-1A cells (Fig. 4h–k). Taken together, these findings demonstrated that GGTLC1 expression was downregulated, which prevented EC cells from proliferating and migrating.

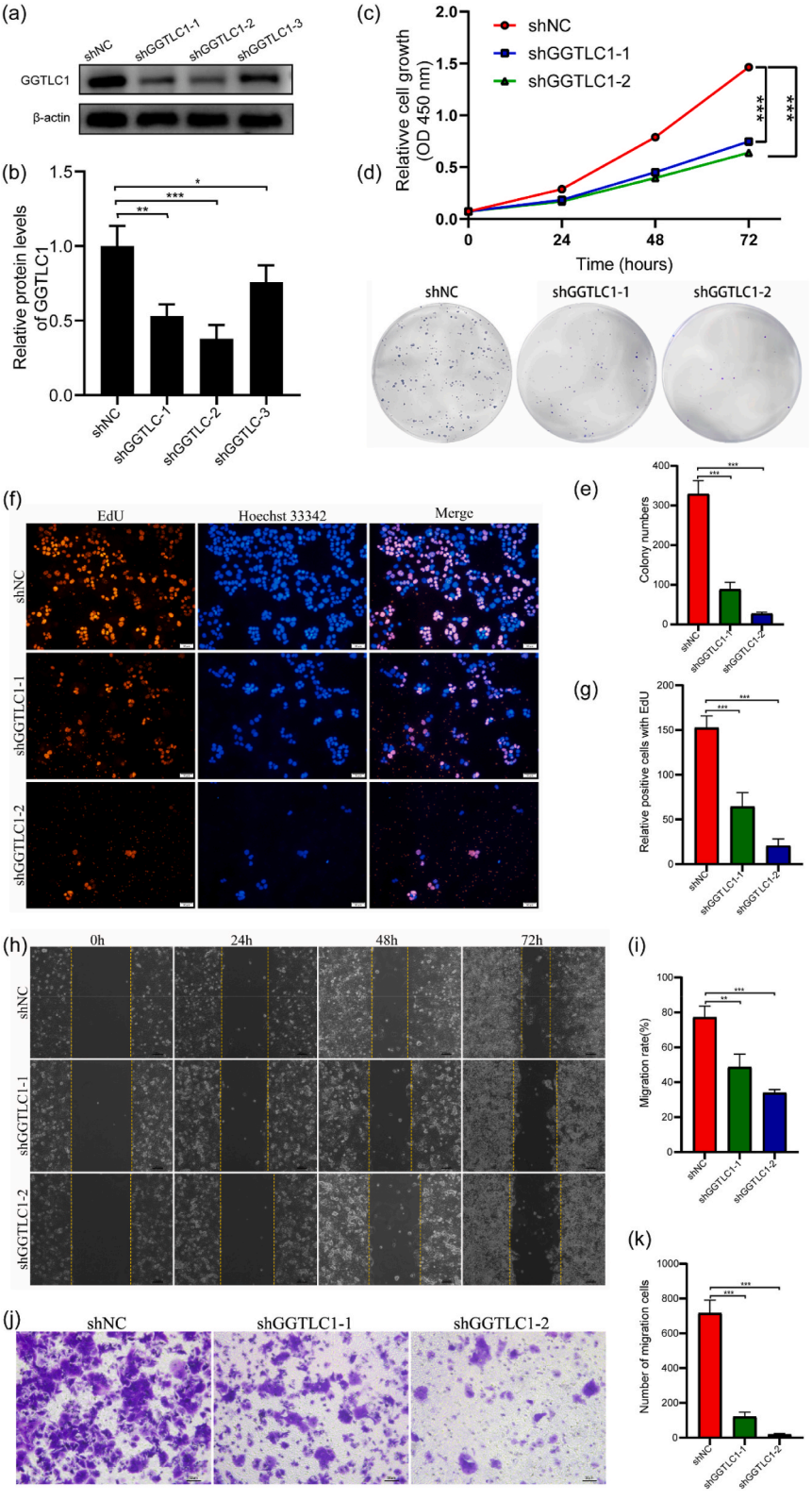


*(caption on next page)*

**Fig. 4.** GGTLC1-shRNA repressed the proliferation and migration of HEC-1A cells. **a, b** GGTLC1 protein expression was lower in shGGTLC1 cells compared to negative control (NC) cells, as detected by western blotting. **c** A time-course study displayed the proliferation of shNC and shGGTLC1 cells, as detected by CCK8 assay. **d, e** GGTLC1 knockdown inhibited colony formation in HEC-1A cells. **f, g** GGTLC1 knockdown inhibited the proliferation of HEC-1A cells, as measured by EdU proliferation assay. **h, i** Silencing GGTLC1 suppressed the migration rate of HEC-1A cells, as measured by wound-healing assay. **j, k** Silencing GGTLC1 suppressed the migration ability of HEC-1A cells using Transwell assay. Each experiment was repeated at least three times, statistical test was applied using one-way analysis of variance test. The scale bars in **f** and **j** measure 50 μm in length, and the scale bar in **h** is 100 μm. The raw data of WB can be found in the supplementary file's Fig. 4(a).

### 3.5. Knockdown of GGTLC1 induces G0/G1 phase arrest and apoptosis in EC

Next, we explored whether cell cycle arrest was linked to the negative effect of GGTLC1 knockdown on cell growth. The number of cells in the G1 phase increased significantly when GGTLC1 was knocked down, whereas the percentage of cells in the S and G2 phases decreased significantly (Fig. 5a–c, j). Meanwhile, western blot results showed that knocking down GGTLC1 resulted in a decrease in cyclinD1 and CDK4 of G1 phase cell cycle proteins (Fig. 5m and n). Moreover, GGTLC1 knockdown notably triggered apoptosis (Fig. 5d–f, k). We used JC-1 staining to detect mitochondrial membrane potential by the flow cytometer. The horizontal axis of FITC-H represented the number of green fluorescent group cells, while the vertical axis of PE-H represented the number of red fluorescent group cells. In healthy cells, normal mitochondrial function triggered red fluorescence, while in apoptotic cells, lowering of mitochondrial membrane potential triggered green fluorescence. The results showed that after knocking down GGTLC1, the number of green fluorescent group cells significantly increased (Fig. 5g–i, l). Subsequently, the western blot results demonstrated that knocking down GGTLC1 resulted in an increase in apoptotic proteins, including caspase3, bax, p21, and a decrease in bcl2 protein (Fig. 5o and p).

### 3.6. Silencing GGTLC1 inhibited the TGF-β/Smad signaling pathway

After knocking down GGTLC1 in HEC-1A cells, DEGs between the experimental group and the control group were obtained through transcriptome sequencing (Fig. 6a and b). The transcriptome sequencing results confirmed the pathway activated by GGTLC1, including TGF-β, Wnt, and Notch signaling pathways (Fig. 6c–e). Considering that TGF-β signaling pathway is widely believed to be involved in tumor cellular growth, movement, and invasion, this pathway was selected for further research. Western blotting was conducted to detect the level of TGF-β and the downstream protein. The level of TGF-β, pSmad2, and pSmad3 proteins in HEC-1A cells were significantly decreased after silencing, but no significant changes in Smad2 and Smad3 proteins were observed (Fig. 6f and g).

### 3.7. Knockdown of GGTLC1 suppresses tumor growth in vivo

Next, we conducted in vivo experiments to confirm the tumor-suppressive role of GGTLC1 silencing, with the results shown in Fig. 7. The volume and size of the tumors originating from HEC-1A cells with stable GGTLC1 knockdown were considerably smaller (Fig. 7a). The same corresponding trend was observed for tumor weight (Fig. 7b). Meanwhile, the tumor volume was monitored every 2–3 days to plot a growth curve. We found that compared to the shNC group, the speeds of tumor growth in the shGGTLC-1/2 groups were dramatically suppressed (Fig. 7c). Accordingly, GGTLC1 knockdown markedly repressed EC tumor growth and proliferation in vivo.

## 4. Discussion

There are approximately 7 % of new instances of EC among women in affluent countries, and it is the most common type of invasive gynecological cancer among women [18]. However, the incidence of EC is still increasing due to the trend of global obesity as well as the progressive aging of our society [19]. Identifying novel diagnostic and therapeutic targets for EC is therefore essential. GGTLC1, as a protein-coding gene, has been rarely studied in cancers, and GGTLC1 was highly expressed in EC cells and human EC tissues in our study. Furthermore, ROC curve analysis suggested that GGTLC1 may be a putative diagnostic biomarker for EC.

The elevated expression of GGTLC1 in EC supports the idea that it may be essential for developing tumors, which is supported by EC cell line research. We found that knocking down GGTLC1 expression mediated by lentivirus vectors induced a decrease in proliferation and migration, as well as induced apoptosis and the arrest in the G0/G1 phase. Based on these results, GGTLC1 is presumed to be a potent tumor-promoting factor in EC.

In this study, we identified the TGF-β/Smad signaling pathway as a downstream pathway of GGTLC1 in EC. Specifically, we demonstrated that knockdown of GGTLC1 inhibits this signaling pathway. Previous studies have highlighted a biphasic role for TGF-β signaling in EC development. Notably, elevated levels of SMAD7 have been shown to accelerate EC progression by inhibiting this pathway [20]. Furthermore, impaired TGF-β signaling, associated with loss of growth inhibition, has been observed in the early stages of EC [21], while enhanced expression of TGF-β is linked to increased cell proliferation in later stages [22], corroborating the findings of our current investigation. The TGF-β pathway is critically involved in regulating cell cycle and apoptosis [23]. In our study, knockdown of GGTLC1 in EC cells was shown to induce G0/G1 phase arrest and apoptosis, underscoring the significance of GGTLC1 as a key regulator of these cellular processes in EC.

Furthermore, enrichment analyses were conducted to explore the gene functions and pathways associated with GGTLC1. Notably, our findings indicated significant enrichment in GO categories such as fatty acid derivative metabolic processes and glucuronate

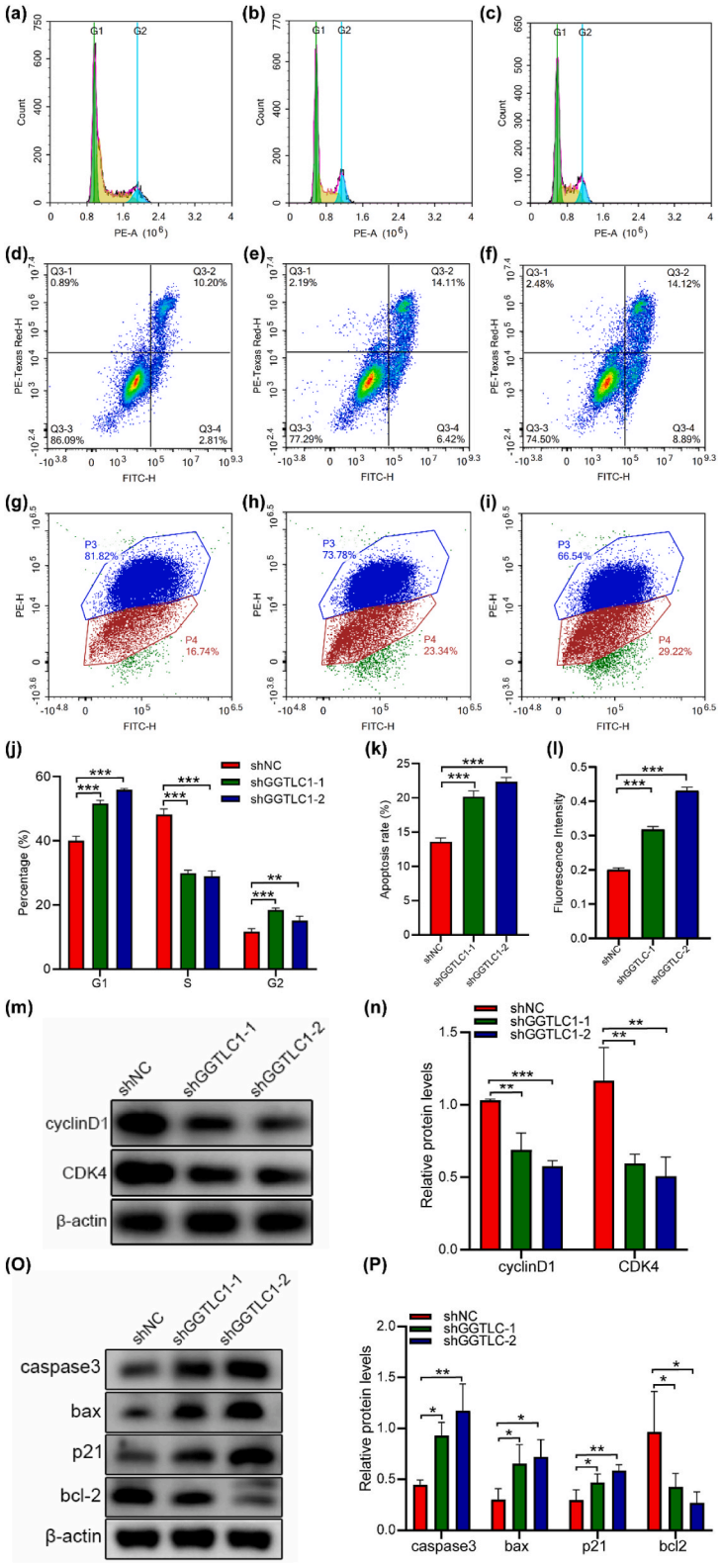


*(caption on next page)*

**Fig. 5.** Impact of GGTLC1 knockdown on the cell cycle, apoptosis and the mitochondrial membrane potential in HEC-1A cells. **a-c, j** Cell cycle progression was determined by flow cytometry. **d-f, k** Apoptosis was determined by flow cytometry. **g-i, l** The mitochondrial membrane potential was determined by flow cytometry. **m, n** Protein levels of cyclinD1 and CDK4 were measured by western blot. **o, p** Protein levels of caspase3, bax, p21, and bcl2 were measured by western blot. Each assay was performed in triplicate. The raw data of WB can be found in the supplementary file's Fig. 5(m) and (o).

metabolic processes, both of which have previously been linked to EC pathophysiology [24]. KEGG pathway analysis highlighted the critical roles of steroid hormone biosynthesis and cytochrome P450 metabolism. Sex steroid hormones are crucial in the pathophysiology of EC [25]. Specifically, cholesterol is converted into pregnenolone by mitochondrial cytochrome P450 enzymes, initiating the biosynthesis of steroid hormones like estrogen and progesterone, which are pivotal in EC development [26]. Additionally, the initial hydroxylation step in estrogen metabolism is catalyzed by cytochrome P450 enzymes [27]. Collectively, these results underscore the crucial involvement of cytochrome P450 and steroid hormones in the molecular mechanisms driving EC.

The methylation of DNA promoter regions represents a significant epigenetic process that is crucial to the development of cancer. In accordance with this, abnormal DNA methylation is an early step during EC development [28]. According to our research, the variation in GGTLC1 methylation levels was significant, while the methylation site cg05002642 and survival probability were significantly correlated. To some extent, hypomethylated GGTLC1 may serve as a factor in assessing prognostic confidence.

Growing evidence has suggested that immune cells play a major and complex role in tumor progression [29–31]. A previous investigation revealed the gene GGTLC1 as a potential immune pathway mediator of treatment resistance in breast cancer [14]. Therefore, we investigated the potential connection between GGTLC1 and immune cells that further penetrate EC. Th1 and Th2 are the two primary types of $CD4^+$ T lymphocytes, and the balance of the two is crucial to the control of the immune response to tumors [32]. Our research revealed that the infiltration of Tgds, T helper cells, Th1 cells, and Th2 cells was adversely correlated with GGTLC1 overexpression, suggesting that GGTLC1 influences EC immunity by controlling immune cell invasion. According to the previous study, establishing a balance between Th1-high and Th1-low is important for reaching a favorable outcome for cancer [33]. Previous research has also suggested that some malignancies are accelerated by an imbalance of helper T cells, cytotoxic T cells, or Th1/Th2 subsets [34,35]. Tgd cells are a unique subgroup of $CD3^+$ T cells that support the body's defense mechanisms against cancer [36,37]. This research may provide a novel immunotherapy target for predicting EC.

Our study, however, is not without limitations. Firstly, we did not conduct rescue experiments by applying inhibitor of the TGF-β/Smad pathway after overexpressing GGTLC1 to see if this could reverse cell function. Secondly, we did not experimentally validate the promoter methylation profile in EC cell lines, such as using molecular biology methods to verify this finding. Thirdly, we did not further evaluate the interaction between GGTLC1 and immune cell infiltration through experiments. These regrets will be addressed in our future research, in order to enable GGTLC1 to be applied as a targeted therapy for endometrial cancer as soon as possible, and to transform basic research into clinical application.

## 5. Conclusions

In conclusion, our research identified a novel method by which GGTLC1 knockdown hindered EC development via the TGF-β/Smad signaling pathway and proved a statistical relationship between GGTLC1 expression and DNA methylation and immune cell infiltration in EC. According to our research, GGTLC1 may be a novel treatment target for EC.

## Funding

This research did not receive any specific funding.

## Ethics statement

This study was reviewed and approved by ethics committee of Lanzhou University School of Basic Medicine, with the approval number: jcyxy20220225. And the ethics approval date was 2022-02-22. We confirmed that the study followed STROBE guidelines and all patients provided "Written Informed Consent" to participate in the study. Animal experiments in this study have been carried out in accordance with either the U.K. Animals (Scientific Procedures) Act, 1986 and associated guidelines, the European Communities Council Directive 2010/63/EU or the National Institutes of Health – Office of Laboratory Animal Welfare policies and laws. All animal studies complied with ARRIVE guidelines.

## Data availability statement

The data generated during and/or analyzed during the current study are available from the corresponding author on reasonable request.

## CRediT authorship contribution statement

**Xiaolin Tang:** Writing – review & editing, Writing – original draft, Visualization, Validation, Supervision, Software, Resources,

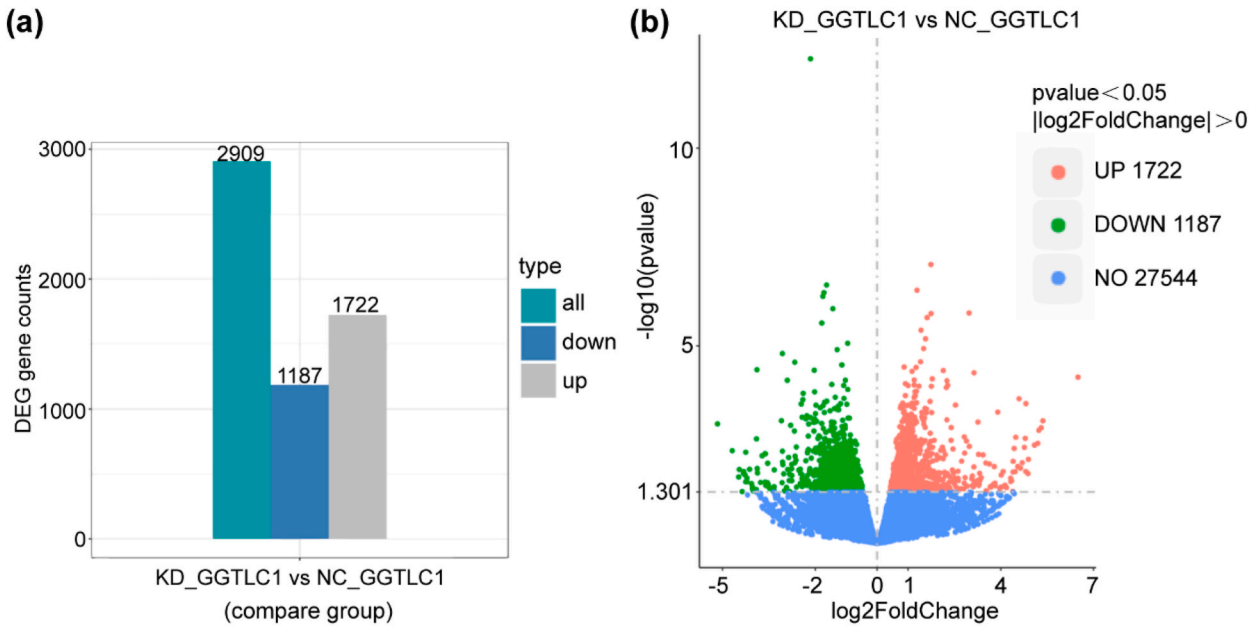


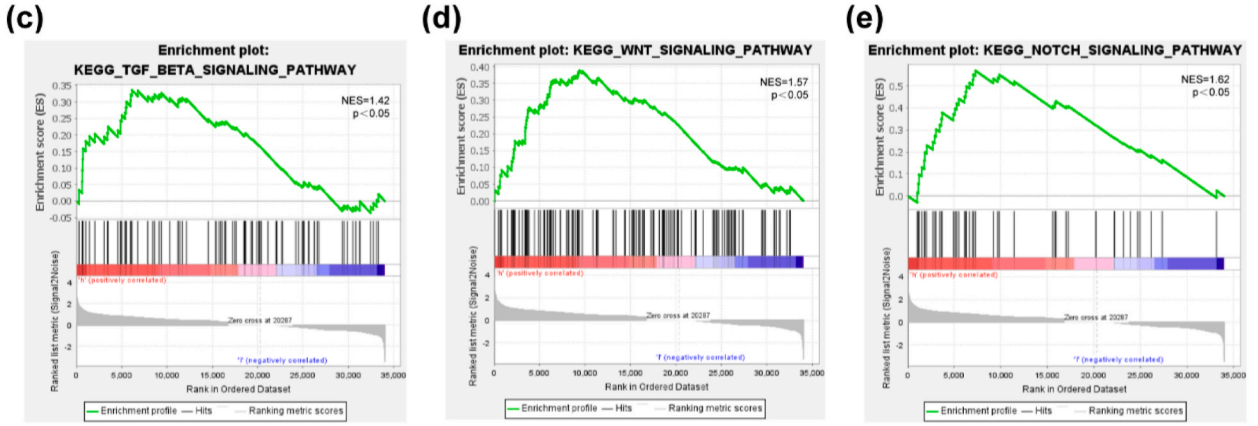


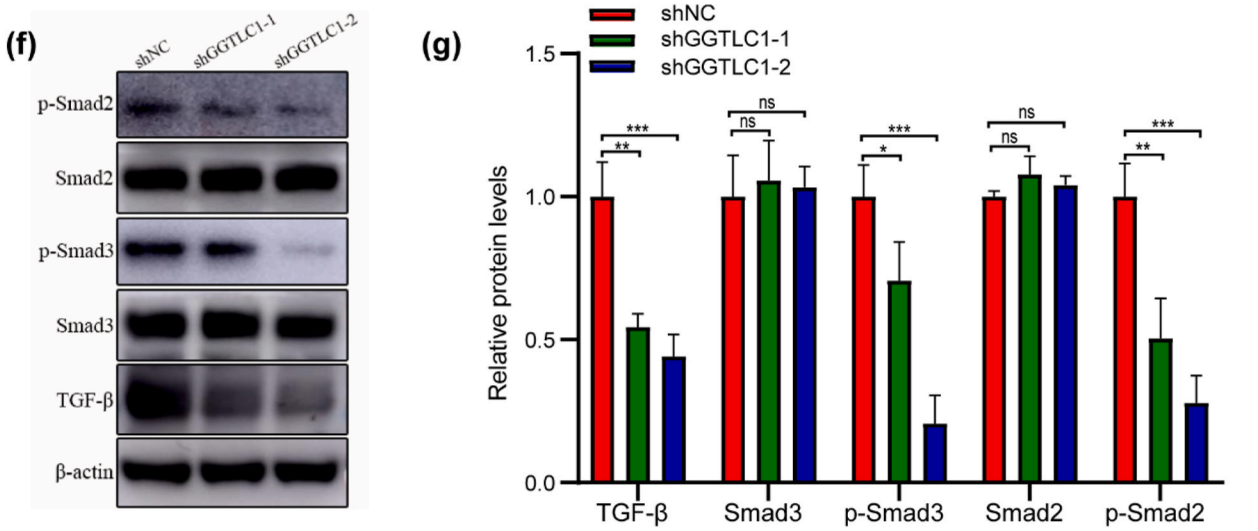


*(caption on next page)*

**Fig. 6.** Silencing of GGTLC1 inhibits the TGF-β/Smad signaling pathway. **a, b** Histograms and volcano plots of DEGs obtained from transcriptome sequencing. **c-e** Pathways activated by GGTLC1 in EC that were obtained by GSEA analysis follwing the transcriptome sequencing. **f, g** Protein levels of TGF-β, pSmad2, Smad2, pSmad3 and Smad3 were measured by western blot. Each experiment was repeated at least three times, statistical test was applied using one-way analysis of variance test. The raw data of WB can be found in the supplementary file's Fig. 6(f).

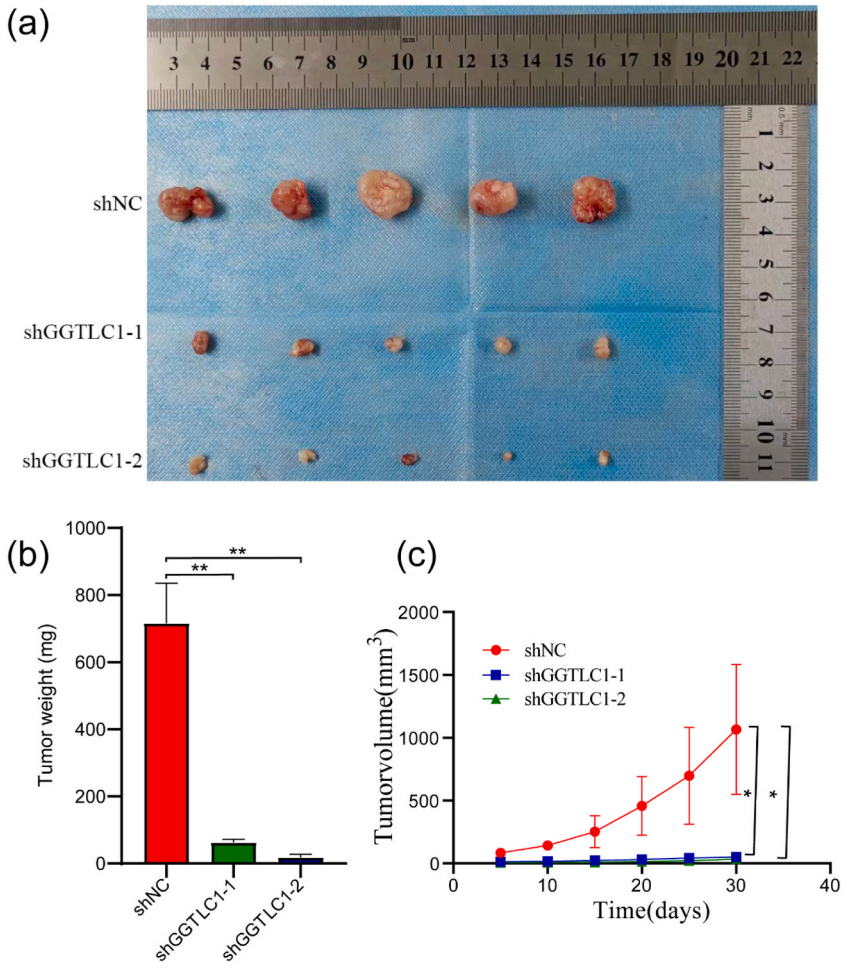


**Fig. 7.** GGTLC1-shRNA repressed tumor growth in nude mice. **a** Photograph of the resected tumor mass after the killing of nude mice. **b** The transplanted tumors were weighed after tumor resection. **c** Tumor volume curve plotted by live measurement of the tumor volume in each group over time. In vivo experiment was conducted using 5 mice per group, statistical test was applied using one-way analysis of variance test.

Project administration, Methodology, Investigation, Formal analysis, Data curation, Conceptualization. **Xuehan Bi:** Writing – review & editing, Methodology, Investigation. **Aihong Yang:** Writing – review & editing, Methodology, Investigation. **Qinganzi Wang:** Writing – review & editing, Software, Methodology, Data curation. **Yongxiu Yang:** Writing – review & editing, Supervision, Conceptualization.

## Declaration of competing interest

The authors declare that they have no known competing financial interests or personal relationships that could have appeared to influence the work reported in this paper.

## Appendix A. Supplementary data

Supplementary data to this article can be found online at https://doi.org/10.1016/j.heliyon.2024.e31973.

## References


[1] R.L. Siegel, K.D. Miller, H.E. Fuchs, A. Jemal, CA cancer J Clin, Cancer Statistics 71 (2021. 2021) 7–33, https://doi.org/10.3322/caac.21654.
[2] F. Bray, J. Ferlay, I. Soerjomataram, R.L. Siegel, L.A. Torre, et al., CA Cancer J Clin. Global cancer statistics 2018, GLOBOCAN estimates of incidence and mortality worldwide for 36 cancers in 185 countries 68 (2018) 394–424, https://doi.org/10.3322/caac.21492.
[3] E. Weiderpass, J. Antoine, F.I. Bray, J.K. Oh, M. Arbyn, Eur J cancer, Trends in corpus uteri cancer mortality in member states of the European Union 50 (2014) 1675–1684, https://doi.org/10.1016/j.ejca.2014.02.020.
[4] C.R. Washington, A. Haggerty, W. Ronner, P.M. Neff, E.M. Ko, Gynecol oncol, Knowledge of endometrial cancer risk factors in a general gynecologic population 158 (2020) 137–142, https://doi.org/10.1016/j.ygyno.2020.03.032.
[5] N. Heisterkamp, J. Groffen, D. Warburton, T.P. Sneddon, Hum Genet. The Human Gamma-Glutamyltransferase Gene Family, vol. 123, 2008, pp. 321–332, https://doi.org/10.1007/s00439-008-0487-7.
[6] S.K. Kunutsor, T.A. Apekey, M. Van Hemelrijck, G. Calori, G. Perseghin, Int J Cancer. Gamma glutamyltransferase, alanine aminotransferase and risk of cancer: systematic review and meta-analysis 136 (2015) 1162–1170, https://doi.org/10.1002/ijc.29084.
[7] K. Takemura, P.G. Board, F. Koga, Antioxidants (basel). A systematic review of serum gamma-glutamyltransferase as a prognostic biomarker in patients with genitourinary, Cancer 10 (2021) 549, https://doi.org/10.3390/antiox10040549.
[8] J. Fu, L. Lu, M. Li, Y. Guo, M. Han, et al., A gamma-glutamyl transpeptidase (GGT)-Triggered charge reversal drug-delivery system for cervical cancer treatment: in vitro and In Vivo Investigation 15 (2023) 1335, https://doi.org/10.3390/pharmaceutics15051335.
[9] J. Kral, S. Jelinkova, P. Zemankova, M. Vocka, M. Borecka, et al., Oncol Lett. Germline Multigene Panel Testing of Patients with Endometrial Cancer, vol. 25, 2023, p. 216, https://doi.org/10.3892/ol.2023.13802.
[10] Z. Shao, Y. Xu, X. Zhang, C. Zou, R. Xie, Strahlenther Onkol, Changes in Serum Uric Acid, Serum Uric Acid/serum Creatinine Ratio, and Gamma-Glutamyltransferase Might Predict the Efficacy of Neoadjuvant Chemoradiotherapy in Patients with Locally Advanced Rectal Cancer, 2023, https://doi.org/10.1007/s00066-023-02096-4.
[11] M. Catalano, G. Roviello, G. Aprile, M. Ramello, R. Conca, et al., Future Oncol. Prognostic value of alkaline phosphatase and gamma-glutamyl transferase in patients with metastatic pancreatic cancer 19 (2023) 937–946, https://doi.org/10.2217/fon-2023-0137.
[12] Z. Xie, T. Kawasaki, H. Zhou, D. Okuzaki, N. Okada, et al., Front pharmacol. Targeting GGT1 eliminates the tumor-promoting effect and enhanced immunosuppressive function of myeloid-derived suppressor cells caused by G-CSF 13 (2022) 873792, https://doi.org/10.3389/fphar.2022.873792.
[13] A. Bansal, D.J. Sanchez, V. Nimgaonkar, D. Sanchez, R. Riscal, et al., Mol Cancer Res. Gamma-Glutamyltransferase 1 Promotes Clear Cell Renal Cell Carcinoma Initiation and Progression 17 (2019) 1881–1892, https://doi.org/10.1158/1541-7786.MCR-18-1204.
[14] Y. Du, Y. Han, X. Wang, H. Wang, Y. Qu, et al., Front Oncol, Identification of Immune-Related Breast Cancer Chemotherapy Resistance Genes via Bioinformatics Approaches 12 (2022) 772723, https://doi.org/10.3389/fonc.2022.772723.
[15] R. Derynck, S.J. Turley, R.J. Akhurst, Nat rev clin oncol, TGFbeta biology in cancer progression and immunotherapy 18 (2021) 9–34, https://doi.org/10.1038/s41571-020-0403-1.
[16] L. Wang, T. Zhuang, F. Li, W. Wei, Environ Sci Pollut Res Int. Fluorene-9-bisphenol inhibits epithelial-mesenchymal transition of human endometrial cancer Ishikawa cells by repressing TGF-beta signaling pathway 26 (2019) 27407–27413, https://doi.org/10.1007/s11356-019-05184-0.
[17] L.J. Cao, Y.J. Zhang, S.Q. Dong, X.Z. Li, X.T. Tong, et al., J Exp Clin Cancer Res. ATAD2 interacts with C/EBPbeta to promote esophageal squamous cell carcinoma metastasis via TGF-beta1/Smad3 signaling 40 (2021) 109, https://doi.org/10.1186/s13046-021-01905-x.
[18] T.A. O'Mara, D.M. Glubb, F. Amant, D. Annibali, K. Ashton, et al., Nat Commun. Identification of nine new susceptibility loci for endometrial cancer 9 (2018) 3166, https://doi.org/10.1038/s41467-018-05427-7.
[19] E.J. Crosbie, S.J. Kitson, J.N. Mcalpine, A. Mukhopadhyay, M.E. Powell, et al., Lancet (London, England), Endometrial cancer. 399 (2022) 1412–1428, https://doi.org/10.1016/S0140-6736(22)00323-3.
[20] X. Li, X. Wu, Onco Targets Ther. MiR-21-5p promotes the progression of non-small-cell lung cancer by regulating the expression of SMAD7 11 (2018) 8445–8454, https://doi.org/10.2147/OTT.S172393.
[21] T.V. Parekh, P. Gama, X. Wen, R. Demopoulos, J.S. Munger, et al., Cancer Res. Transforming growth factor beta signaling is disabled early in human endometrial carcinogenesis concomitant with loss of growth inhibition 62 (2002) 2778–2790.
[22] A. Sapir, J. Choi, E. Leikina, O. Avinoam, C. Valansi, et al., Dev Cell. AFF-1, a FOS-1-regulated fusogen, mediates fusion of the anchor cell in C. elegans 12 (2007) 683–698, https://doi.org/10.1016/j.devcel.2007.03.003.
[23] J. Wang, Z. Xu, Z. Wang, G. Du, L. Lun, Cytokine. TGF-beta signaling in cancer radiotherapy 148 (2021) 155709, https://doi.org/10.1016/j.cyto.2021.155709.
[24] P. Li, B. Shan, K. Jia, F. Hu, Y. Xiao, et al., BMC Cancer. Plasma omega-3 polyunsaturated fatty acids and recurrence of endometrial, cancer 20 (2020) 576, https://doi.org/10.1186/s12885-020-07035-5.
[25] L. Thakur, S. Thakur, Front. Endocrinol. The interplay of sex steroid hormones and microRNAs in endometrial cancer: current understanding and future directions 14 (2023) 1166948, https://doi.org/10.3389/fendo.2023.1166948.
[26] Y.X. Zhou, J. Wei, G. Deng, A. Hu, P.Y. Sun, et al., Nat Cell Biol. Delivery of low-density lipoprotein from endocytic carriers to mitochondria supports steroidogenesis 25 (2023) 937–949, https://doi.org/10.1038/s41556-023-01160-6.
[27] Y. Tsuchiya, M. Nakajima, T. Yokoi, Cancer Lett. Cytochrome P450-mediated metabolism of estrogens and its regulation in human 227 (2005) 115–124, https://doi.org/10.1016/j.canlet.2004.10.007.
[28] N. Wentzensen, J.N. Bakkum-Gamez, J.K. Killian, J. Sampson, R. Guido, et al., Int J Cancer. Discovery and validation of methylation markers for endometrial, cancer 135 (2014) 1860–1868, https://doi.org/10.1002/ijc.28843.
[29] X. Liu, D. Feng, W. Wang, J. Liang, H. Yu, et al., J Immunother, Tumor microenvironment CD8 T and treg cells-related genes signature distinguishes distinct prognosis and targeted therapies response in endometrial, Cancer 46 (2023) 178–191, https://doi.org/10.1097/CJI.0000000000000463.
[30] C. Meijuan, X. Meng, L. Fang, W. Qian, J Ovarian Res. Synaptotagmin-like Protein 1 Is a Potential Diagnostic and Prognostic Biomarker in Endometrial Cancer Based on Bioinformatics and Experiments, vol. 16, 2023, p. 16, https://doi.org/10.1186/s13048-023-01097-2.
[31] K. Dessources, L. Ferrando, Q.C. Zhou, A. Iasonos, N.R. Abu-Rustum, et al., Gynecol Oncol. Impact of immune infiltration signatures on prognosis in endometrial carcinoma is dependent on the underlying molecular subtype 171 (2023) 15–22, https://doi.org/10.1016/j.ygyno.2023.01.037.
[32] X. Yin, S. Chen, S.C. Eisenbarth, Annu Rev Immunol. Dendritic Cell Regulation of T Helper Cells, vol. 39, 2021, pp. 759–790, https://doi.org/10.1146/annurev-immunol-101819-025146.
[33] B. Mahata, X. Zhang, A.A. Kolodziejczyk, V. Proserpio, L. Haim-Vilmovsky, et al., Cell Rep. Single-cell RNA sequencing reveals T helper cells synthesizing steroids de novo to contribute to immune homeostasis, vol. 7, 2014, pp. 1130–1142, https://doi.org/10.1016/j.celrep.2014.04.011.
[34] K. Wang, T. Shen, G.P. Siegal, S. Wei, Hum Pathol. The CD4/CD8 ratio of tumor-infiltrating lymphocytes at the tumor-host interface has prognostic value in triple-negative, Breast Cancer 69 (2017) 110–117, https://doi.org/10.1016/j.humpath.2017.09.012.
[35] M. Tosolini, A. Kirilovsky, B. Mlecnik, T. Fredriksen, S. Mauger, et al., Cancer Res. Clinical impact of different classes of infiltrating T cytotoxic and helper cells (Th1, th2, treg, th17) in patients with colorectal, cancer 71 (2011) 1263–1271, https://doi.org/10.1158/0008-5472.CAN-10-2907.
[36] N.L. De Vries, J. Van De Haar, V. Veninga, M. Chalabi, M.E. Ijsselsteijn, et al., Nature. Gammadelta T Cells Are Effectors of Immunotherapy in Cancers with HLA Class I Defects, vol. 613, 2023, pp. 743–750, https://doi.org/10.1038/s41586-022-05593-1.
[37] V. Catros, O. Toutirais, F. Bouet, F. Cabillic, M. Desille, et al., Med Sci (Paris). [Tgammadelta lymphocytes in oncology: unconventional killer lymphocytes] 26 (2010) 185–191, https://doi.org/10.1051/medsci/2010262185.